ORIGINAL ARTICLE

Improvement of salt gradient solar ponds' performance using nanoparticles inside the storage layer

Hossein Beiki[1] · Ehsan Soukhtanlou[2]

Abstract

The solar pond is one of the usual tools used for solar energy harvesting in the world, although its low efficiency is still a big challenge. In this study, to enhance the thermal efficiency of the laboratory-scale salinity gradient solar pond, three different nanoparticles, i.e., SiO_2, Fe_3O_4, and ZnO, were dispersed into a salt-water solution as the based liquid. Nanoparticles' mass concentrations used in the based liquid were 0.012%, 0.036%, and 0.06%. The simulated sunlight thermal energy was supplied by a 500 W halogen lamp. The prepared nanofluids were used as lower layer of the pond. Approximately 3 days after filling the pond, the stable salinity gradient was formed and after almost 2 days of exposure to the simulated sunlight, the temperature of the pond layers reached thermal equilibrium. The results showed that lower layer temperature increased continuously with nanoparticles' concentration, for all nanofluids. Based on the measured temperature, the pond thermal performance was calculated, showing that all mentioned nanoparticles could enhance the thermal efficiency of the SGSP. The maximum lower layer temperature (~ 47 °C) and thermal efficiency enhancement ratio (35.13%) were obtained for the 0.06% ZnO nanofluid. This nanofluid showed the minimum light scattering (particle size parameter = 0.248) and transmittance (near zero) over the UV–Vis wavelength, leading to the increased thermal efficiency of the pond, as compared to the SiO_2 and Fe_3O_4 nanofluids. In addition, using nanoparticles, the time required to reach equilibrium conditions in the pond was decreased, with the maximum of about 9 h.

Keywords Salt gradient solar pond · Nanoparticles · Heat storage layer · Thermal efficiency

Introduction

Due to the industrial development and the rapid growth of human population, consumption of fossil fuels such as natural gas is increasing. On the other hand, the high cost of energy carriers, limitations in the use of fossil fuels, and the growing environmental pollution have encouraged researchers to find an alternative and new clean energy resource (Beiki et al. 2009; Keramati and Beiki 2017). Energy crisis, which has raised concerns about the future of the world, can be solved using renewable energy resources such as solar energy and modifying the consumption patterns.

One of the inexhaustible, clean and cheap renewable energies is the solar energy. It is of interest to the world due to its many benefits. There are various solar systems such as solar pond (Alcaraz et al. 2016; Ziapour et al. 2016; Abdullah et al. 2016; Elsarrag et al. 2016), solar still (Rajaseenivasan et al. 2013), solar heater (Tsilingiris 1996; Mahian et al. 2013), and solar collector (Said et al. 2013; Milanese et al. 2016; Qarony et al. 2018; Karuppuchamy et al. 2013; Gulzar et al. 2018) for capturing and converting solar energy into other energies, namely, thermal energy or electricity, which are suitable for human uses. One of the most widely used equipment to collect and store solar energy is the solar ponds; they can be used for heating, cooling, water desalination, or electricity generation (Rajaseenivasan et al. 2013; Abdullah et al. 2016; Elsarrag et al. 2016; Bozkurt et al. 2015; Liu et al. 2015; Assari et al. 2015; Michael and Iniyan 2015; Salata and Coppi 2014; Tsilingiris 1996). Among them, salinity gradient solar ponds (SGSPs) are one of the most common because of their stability and prevention of convection current from the bottom to the top of the

✉ Hossein Beiki
  hbeiki@qiet.ac.ir

1 Department of Chemical Engineering, Quchan University of Technology, Quchan, Iran

2 Department of Mechanical Engineering, Engineering Faculty, Ferdowsi University of Mashhad, Mashhad, Iran

pool due to the strong salt concentration gradient achieved using mineral salts such as NaCl (Abdullah et al. 2016; Kho et al. 1991; Li et al. 2000), Na_2CO_3 (Kurt et al. 2006; Lund and Keinonen 1984), KNO_3 (Leshuk et al. 1978; Subhakar and Murthy 1994; Lund and Keinonen 1984), $MgCl_2$ (Lund and Keinonen 1984; Keren et al. 1993; Subhakar and Murthy 1991), etc. (Lund and Keinonen 1984; Hassairi et al. 2001; Murthy and Pandey 2003; Pawar and Chapgaon 1995; Banat et al. 1994). Therefore, it is very essential to conduct research on such solar ponds. An SGSP is a pool of salty water which collects and stores the solar radiation. These solar ponds contain three layers of saltwater with different densities. The absorbed sun's light energy is extracted from a storage layer (the bottom layer of the solar pond), whose temperature reaches up to 60 °C (Mahian et al. 2013) or more (if the pond walls are perfectly insulated), and can be used for power generation, heating and salt-water desalination without any emission of greenhouse gases.

There is already a considerable body of the literature regarding the problem of designing, modeling, and constructing SGSPs. Liu et al. (2015) experimentally and numerically investigated the thermal performance of the mini-trapezoidal solar pond. Their numerical results showed that the temperature of the trapezoidal solar pond was about 5 °C higher than that in the rectangular one. In addition, heat losses from the lower layer decreased in the trapezoidal structure. Similarly, the effect of the solar pond cross-sectional structure on heat storage was also investigated by Assari et al. (2015). They demonstrated that the maximum temperature in the rectangular cross-sectional pond was 3 °C higher than that in the circular one. The stability of Na_2CO_3 solar pond was investigated by Kurt et al. (2006). Their results revealed that convection from the bottom to the surface of the solar pond was suppressed by density gradient achieved using Na_2CO_3 salt. They noted that to store heat in the pond, a density gradient with a 12% salinity range from the bottom to the surface of the solar pond was necessary. Temperature distribution in an insulated solar pond was calculated during the day and night times, showing that, depending on the temperature difference, there was a large amount of heat losses between day and night times (Karakilcik et al. 2006). Thermodynamic analysis based on energy and exergy of solar ponds was also investigated (Dehghan et al. 2013; Bozkurt et al. 2015). Dehghan et al. (2013) studied the energetic and exergetic performance of the square and circular cross-sectional solar ponds. They illustrated that the circular cross-sectional pond had a higher thermal performance than the square one. Energy efficiency for the heat storage layer of the circular pond was 2.15% greater than that of the square one.

A major challenge that has caused solar pond not to become commercial is the low efficiency of the heat storage inside its lower layer and conversion of it to thermal energy

or electricity (Rashidi et al. 2017; Karakilcik et al. 2006; Liu et al. 2015). Many researchers have already worked on solar ponds, although the improvement and optimization of the efficiency, performance, and construction of solar ponds are still a challenge for the researchers and designers all over the world. One of the most effective factors that can enhance thermal efficiency in solar ponds related to the thermal and optical properties of the liquids that form the lower layer of the ponds. After the appearance of nanofluids, which are stable suspensions containing nano-sized particles, in recent years, the application of nanoparticles to increase the efficiency of solar systems has been investigated (Chen et al. 2017; Milanese et al. 2016; Rativa and Gómez-Malagón 2015; Michael and Iniyan 2015; Al-Nimr and Al-Dafaie 2014; Mahian et al. 2013; Said et al. 2013; Ladjevardi et al. 2013; Karunamurthy et al. 2012).

The studies addressing the effects of nanoparticles on the performance of solar systems are chiefly related to solar collector devices (Mahian et al. 2013). The majority of the studies in this field have shown that using nanoparticles, the thermal performance of solar collectors could be increased (Mahian et al. 2013; Tyagi et al. 2009). To increase the solar absorption efficiency, the thermal energy of visible and infrared region lights must be absorbed by tuning the fluids' optical properties. Metallic, metallic oxide, carbon nanotubes, graphite, and graphene were added to usual fluids to promote their optical properties. Rose et al. (2017) deduced that the solar radiation absorbance of the ethylene glycol/graphene oxide nanofluids increased with concentration of nanoparticles. The authors have shown that the 0.012 vol% nanofluid could be suitable to achieve the maximum absorption and the least reflectance over the visible wavelength. Optical properties of metal oxide nanoparticles, namely, ZnO, CeO_2, and Fe_2O_3, in gas-based nanofluids, which are nanoparticles mixed with a gas basis such as Air, N_2, He, etc., have been measured, showing that for high temperature applications, up to 500 °C, and the absorption coefficient of nanoparticles could not be changed significantly (Milanese et al. 2016). Therefore, gas-based nanofluids containing metal oxide nanoparticles could be suitable for use as the working fluid in the concentrated solar power plants (Milanese et al. 2016). Many investigations have been carried out to probe the effect of nanoparticles effect on the thermal efficiency of solar collectors, while studies on the applications of nanofluids inside the solar pond layers are very limited (Al-Nimr and Al-Dafaie 2014). In reference (Al-Nimr and Al-Dafaie 2014), authors simulated a two-layer nanofluids solar pond. Their results showed that nanofluids increased the thermal efficiency and the storage capacity of the nanofluid pond.

The efficiency of a solar pond depends on the heat losses through its side walls and the bottom and the absorption of the solar radiation. The performance of the solar pond can

be improved with the heat gain from solar radiation. Increasing the absorption coefficient is the most important way to enhance the solar heat gain in the solar pond. Since the nanofluids are a kind of superior heat transfer fluid (Shahmohammadi and Beiki 2016) with good optical properties, the aim of this study was to investigate the effect of nanofluids on the thermal performance of an experimental solar pond.

Based on the literature review, there have been no experimental studies on the use of nanofluids as the lower layer of the solar ponds. However, in this study, we have tried to fill a gap in the literature by investigating the effect of three different types of nanoparticles, i.e., SiO_2, Fe_3O_4, and ZnO supplied by US research nanomaterial (USA), on the thermal performance of a lab-scale solar pond.

Suspensions' preparation and stability

To prepare nanofluids as the working fluid for doing the tests, the two-step method was used. In this method, nanoparticles were gradually added to the saline solution, to avoid granulation (Beiki et al. 2013). By considering water volume in the bottom layer of the pond (5000 mL), suspensions with the mass concentrations of 0.012%, 0.036% and 0.06% were prepared. To make a homogeneous and stable suspension, nanoparticles were added to the base fluid in several steps. At each step of adding nanoparticles, the specimen was mixed by a magnetic stirrer for 22 min, and then, it was kept under ultrasonic vibration (Pars Nahand Co., Iran) for 22 min. In general, each nanofluid was both sonicated by ultrasonic vibrator and mixed by the stirrer for about 3 h. The procedure for preparing nanofluids has been explained extensively in our previous work (Manouchehrian Fard and Beiki 2016; Fard and Beiki 2017).

The properties of the mentioned nanoparticles are listed in Table 1. To characterize the nanofluids containing the mentioned nanoparticles, dynamic light scattering (DLS) analysis (Cordouan Vasco3, France), and the results of Zeta potential (CAD Zeta Compact, France) are shown in Figs. 1 and 2, respectively.

The high absolute magnitude of Zeta potential induces higher stability of nanofluid. According to Fig. 2, the highest absolute value of the Zeta potential belongs to the SiO_2 nanofluids, showing that SiO_2 nanofluids were more stable among the studied nanofluids.

The absorption spectrum and stability of nanofluids containing various types of nanoparticles (i.e., SiO_2, Fe_3O_4, and ZnO) were measured by UV–Vis spectrophotometer (Thermo-Fisher Scientific, USA). The absorbance of nanofluids with three different mass concentrations of nanoparticles is shown in Fig. 3. It is observed that the absorbance of nanofluids increased with nanoparticles concentrations. At the same concentration, ZnO nanofluids had higher absorbance values, as compared to SiO_2 and Fe_3O_4 nanofluids over the UV–Vis spectrum. As can be seen in Fig. 3, the peak value of the absorbance for ZnO, Fe_3O_4, and SiO_2 nanofluids was around 379, 399, and 370 nm, respectively.

According to the Beer–Lambert law, the absorbance and concentration of a sample could have a linear pattern. The Beer–Lambert law is usually written as

$$A = \alpha C x, \tag{1}$$

where A is the absorbance, α is the absorption coefficient depending on the wavelength, C is the concentration of the sample, and x is the light path length.
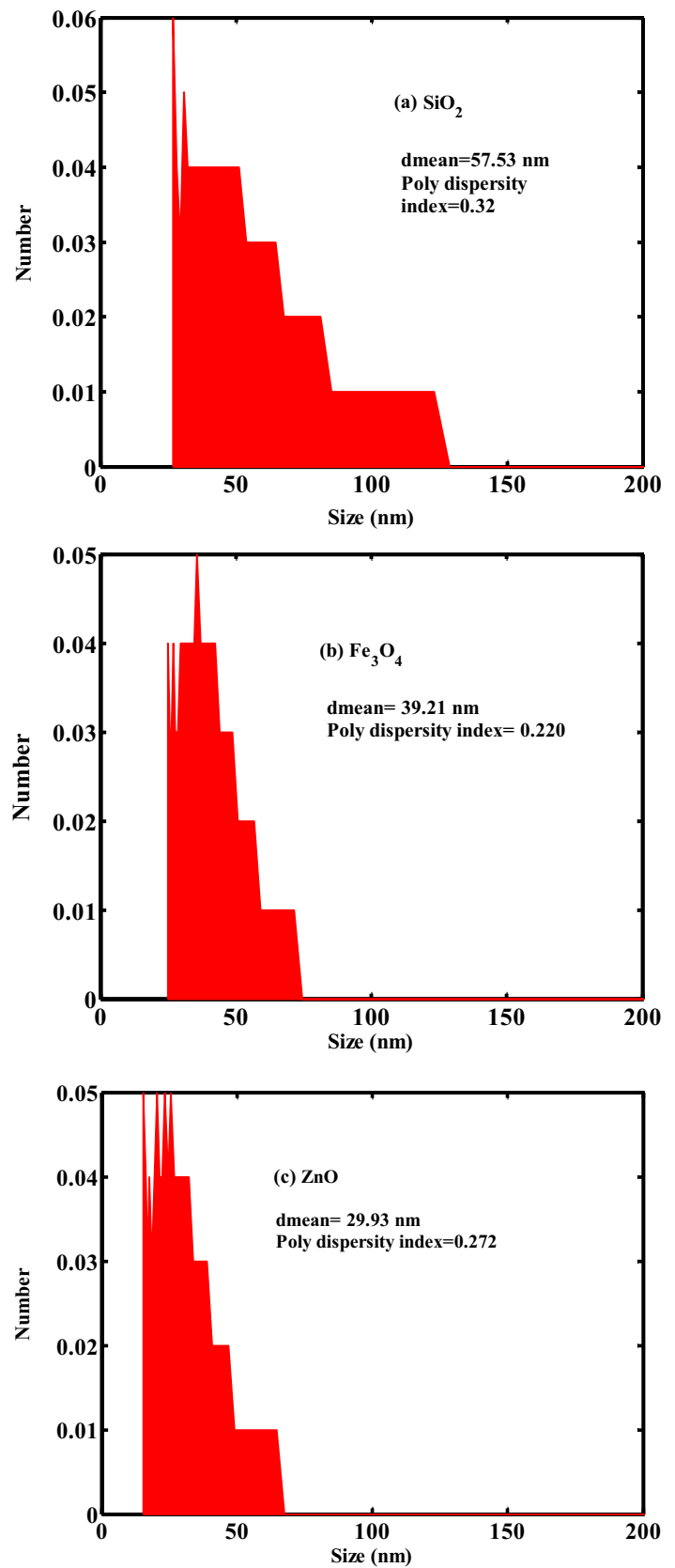
For the purpose of investigating the nanofluids stability, for each nanofluid, six different nanoparticles' concentrations were prepared. Then, the peak value of absorption is measured and is plotted in Fig. 4. Regarding each nanofluid, this figure shows that absorbance–concentration experimental data have a linear trend consistent with the Beer–Lambert law. Using the MATLAB R2014a software, line-fitting was done. Characteristics of the fitted lines (i.e., slopes and intercepts) are listed in Table 2.
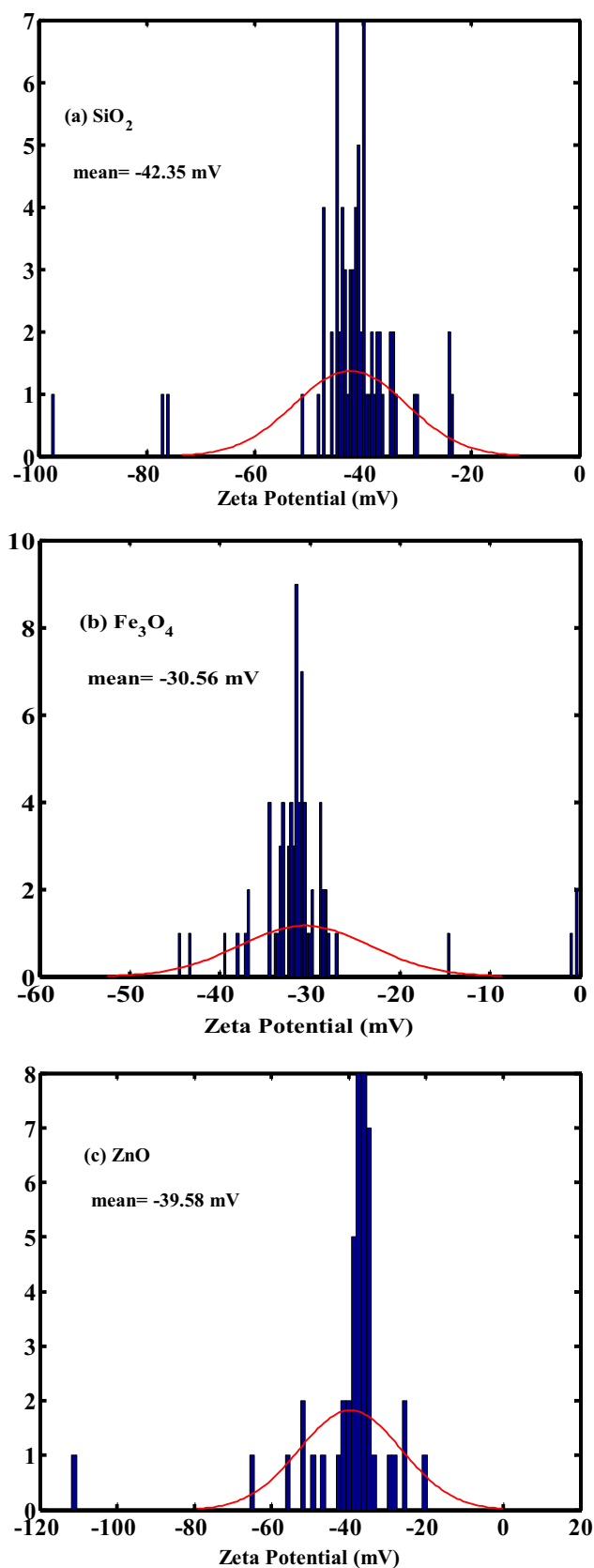
Nanofluids are homogeneous, stable, and dilute colloidal suspensions containing nanoscale particles. A very crucial characteristic of nanofluids is the stability of nanoparticles inside a hosting fluid to create a homogeneous phase. Indeed, homogeneity and stability are the advantages of a nanofluid, as compared to the suspensions containing micro- and millimeter-sized particles. When nanoparticles settle out, the nanofluid is converted from a homogeneous state to a heterogeneous one, and it can no longer be called the nanofluid. The precipitation leads to dropping the nanofluid efficiency due to the decrease in the concentration of nanoparticles dispersed in the base fluid, the increase of the required pumping power, blockage of the channels, and so

Table 1 Specifications of nanoparticles

Nanoparticles (catalog number)	Size (nm)	Specific surface area (m²/g)	Color	Purity	Density (g/cm³)	c_p (J/kg K)	k (W/m K)
SiO_2 (US3438)	20–30	180–600	White	99+%	2.4	710	1.45
Fe_3O_4 (US3220)	20–30	40–60	Dark brown	98+%	5.1	670	80.4
ZnO (US3590)	10–30	20–60	White	99+%	5.606	495.2	13

Fig. 1 DLS analysis of nanofluids in number: **a** SiO$_2$, **b** Fe$_3$O$_4$, **c** ZnO

(a) SiO$_2$

dmean=57.53 nm
Poly dispersity index=0.32

(b) Fe$_3$O$_4$

dmean= 39.21 nm
Poly dispersity index= 0.220

(c) ZnO

dmean= 29.93 nm
Poly dispersity index=0.272

Fig. 2 Zeta-potential diagram for nanofluids: **a** SiO_2, **b** Fe_3O_4, and **c** ZnO

on. In this study, the stability of each nanofluid at the highest concentration (i.e., 0.06%) was measured over 2 weeks after preparation. Figure 5 shows the relative nanoparticles concentration, which is the ratio of the subsequent concentration of the nanofluid to that of the fresh nanofluid. It could be concluded that all nanofluids were stable up to 5 days, with the maximum sedimentation of around 16% for ZnO nanofluids, and less than 10% for the SiO_2 nanofluid. It could be said that all prepared nanofluids were suitable for use in the experimental solar pond, because the solar pond reached the stable layers of salt after 3 days and the thermal equilibrium after 2 days of exposure to light. According to Fig. 5, SiO_2 nanofluid was more stable than other nanofluids. This could also be deduced from the density of the nanoparticles dispersed inside the hosting solution. According to Table 1, ZnO nanoparticles had a higher density when compared to other nanoparticles. Therefore, although ZnO nanoparticles were smaller in size, they were clustered faster due to the higher density and the formation bigger agglomerates with the smaller Brownian motion (Beiki et al. 2013a, b). It is obvious that nanoparticles' clusters are more massive than well-dispersed nanoparticles, leading to the faster precipitation.

According to Fig. 5, for the ZnO nanofluid, the fastest sedimentation occurred (i.e., 28% after 14 days), while the maximum sedimentation of less than 18% was obtained for the SiO_2 nanofluid at the same time. It may be said that, without adding any surfactant, all nanofluids had good stability and dispersion.

Experimental setup and procedures

One of the solar ponds that is widely used on large scale to produce warm water and trap solar energy is SGSP. In general, SGSP consists of three layers (zones). The upper convective zone (UCZ) consists of the least level of salinity (almost 3%) and almost constant temperature closed to ambient temperature. In the lower convective zone (LCZ), the heat is collected and stored. The amount of salinity and temperature are constant and maximum in the LCZ. In the non-convective or gradient zone (NCZ), the temperature and salinity increase from upper to lower layer. Because this layer has enough salinity gradient, heat transfer from the LCZ to the UCZ occurs by conduction instead of convection.

To examine the effect of nanoparticles on the LCZ temperature, an SGSP with the surface area of 33.5×20 cm^2 and the depth of 50 cm was made. Figure 6 shows the schematic diagram of the experimental setup. The SGSP used in this study had been made of a 6 mm glass. To decrease the heat losses from the side walls and the bottom of the pond, using thermal insulations was crucial to reduce the heat transfer from the walls. For this purpose, polyurethane

Fig. 3 UV–Vis spectrum absorption of different concentration of nanofluids: **a** SiO$_2$, **b** Fe$_3$O$_4$, **c** ZnO
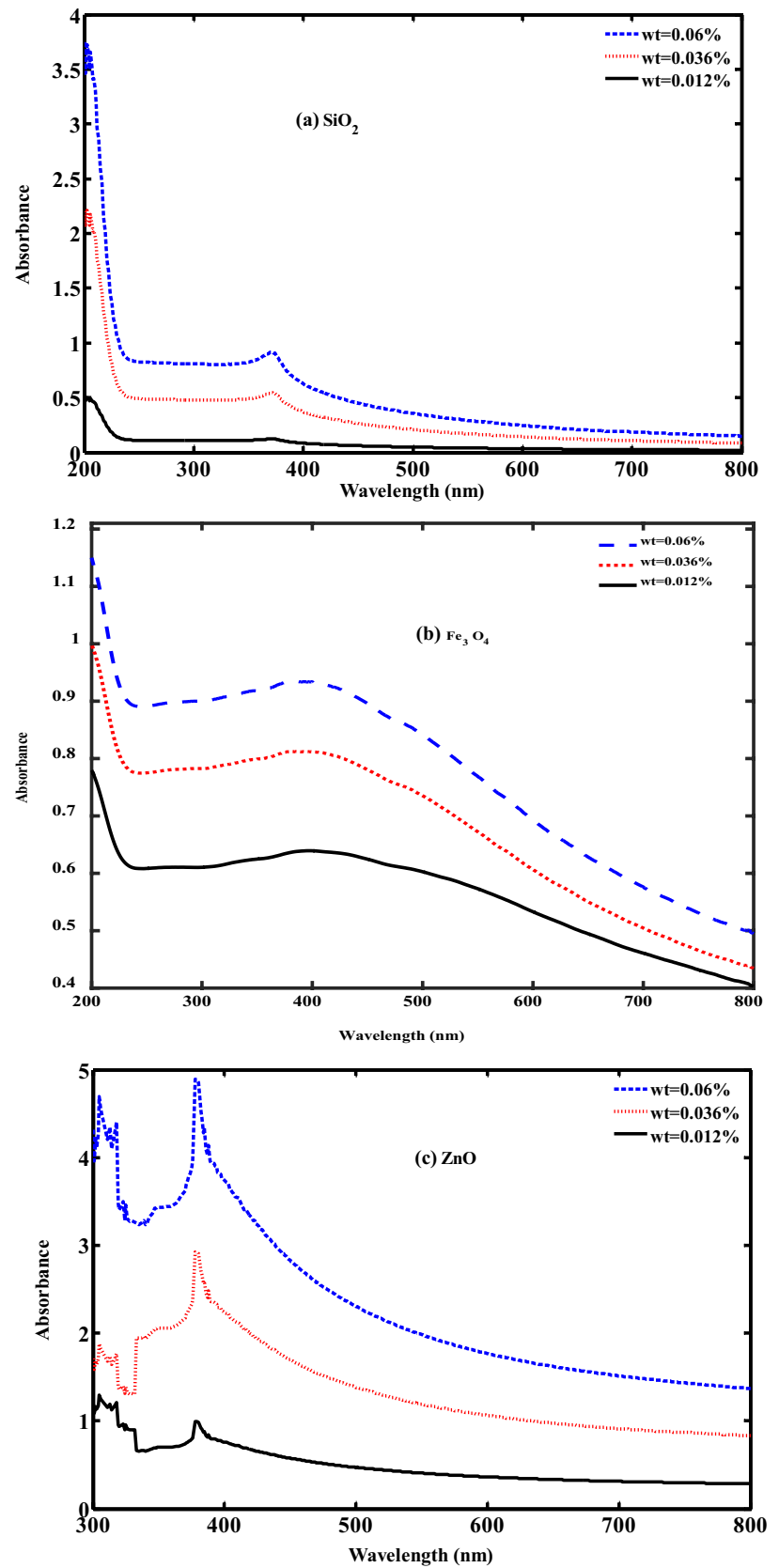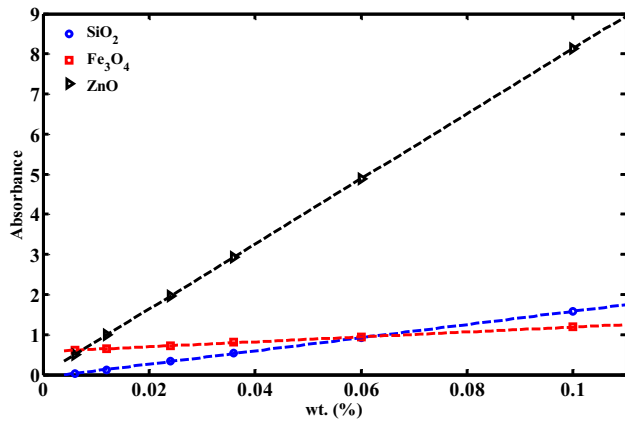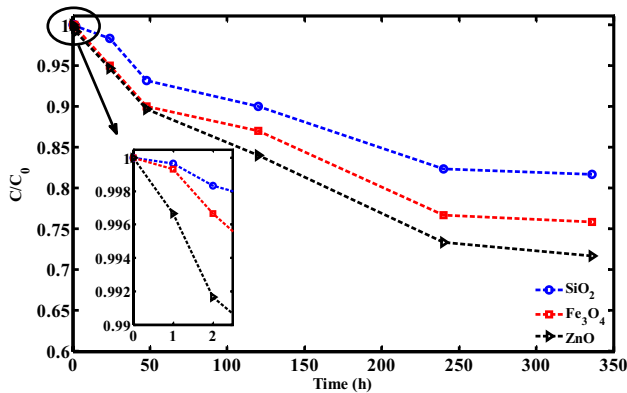
Fig. 4 Experimental absorbance–concentration data and trend lines for each nanofluid

Table 2 Fitted lines' characteristics

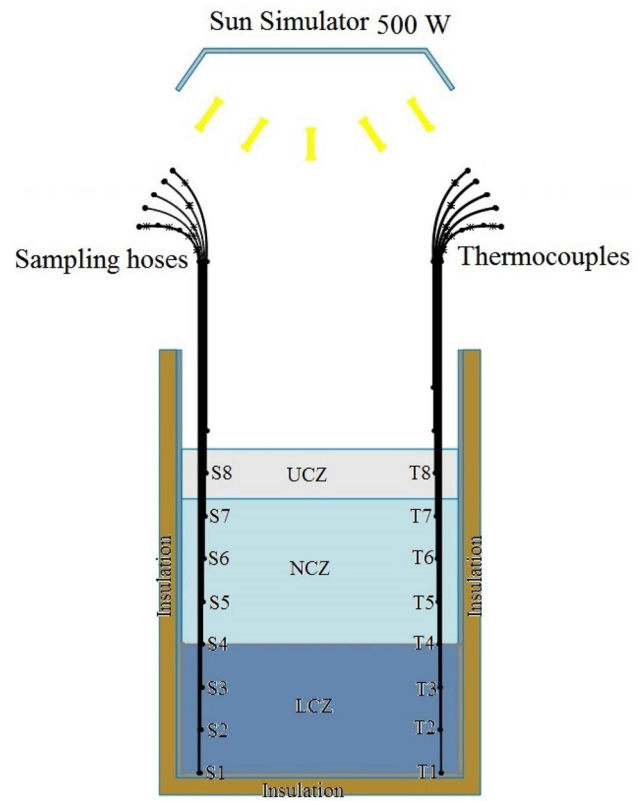| Material type	Slope	Intercept	R^2
SiO$_2$ nanofluids	16.46	− 0.06613	0.9988
Fe$_3$O$_4$ nanofluids	6.131	0.5742	0.9904
ZnO nanofluids	81.21	0.01062	1

Fig. 5 Sedimentation rate for the most concentrated nanofluids (i.e., wt.% = 0.06%) at the stagnation conditions

Fig. 6 Schematic diagram of experimental SGSP (more color intensity equivalent to more salinity concentration)

Table 3 Specifications of the primary layers of the pond

Layer no.	Density (g/cc)	Layer volume (cc)	Thickness (cm)
0	1.22	5000	≈ 8
1	1.17	1700	2.5
2	1.16	1700	2.5
3	1.14	1700	2.5
4	1.13	1700	2.5
5	1.11	1700	2.5
6	1.09	1700	2.5
7	1.08	1700	2.5
8	1.06	1700	2.5
9	1.04	1700	2.5
10	1.03	1700	2.5
11	1	3200	≈ 5

foam was used as a thermal insulation material. A 500 W Osram halogen lamp was used to simulate sunlight in the laboratory. The Sun simulator was located 40 cm above the pond's surface. For the better absorption of radiation, the bottom of the pond was painted black. To measure the density of saltwater and determine the salinity gradient at each 5 cm interval, some hoses were contrived for sampling (S1–S8 in Fig. 6). Eight thermometers (K-Type) were also used to read the temperature with an accuracy of ± 0.1 °C at the same level as the sampling hoses.

To create a salinity gradient in the pond, sodium chloride with a minimum purity of 99.4% (Sodeh, Iran) was used.

To fill the pond, layers with different concentrations of salt should be prepared and slowly added to the pond. In fact, gradually adding layers to the pond would avoid mixing layers. Table 3 shows the layers characteristics. The thickness of the upper, gradient, and storage zones of the SGSP was selected about 5, 25 and 8 cm, respectively.

After filling the pond, the salinity gradient was raised in a stepwise manner; then, upon the passage of time (some days) and the mixing of the salt layers, along with the gradual diffusion of salt to the higher layers, we would have a linear concentration profile. From sampling hoses, some samples were taken from different layers by syringe (10 mL) and the sample density was measured using pycnometer 10 ± 0.2 mL and digital laboratory balance with an accuracy of $\pm 10^{-3}$ g. Each density measurement was done in triplicate, and density values corresponded to the average of three measurements. The maximum standard deviation for three measurements was 0.23%; it was close to the uncertainty value (0.2%) calculated by Eq. (2):

$$E_{M} = \sqrt{\sum_{i=1}^{N} \left(\frac{x_i}{M} \frac{\partial M}{\partial x_i} E_{x_i} \right)^2},\qquad(2)$$

where E_M is the maximum uncertainty in M quantity, N is the number of independent variables (measured quantity), x_i is the independent variable, and E_{xi} is the measurement error in x_i, which is the ratio of the measuring device's accuracy to the minimum amount of measurement.

The changes in the salinity gradient on different days, after filling the pond, are shown in Fig. 7. The salt gradient difference between the upper and lower regions of the pond was about 0.22 g/cm³. The range of the salt gradient difference between the upper and lower regions of the pond in this study is similar to what had been reported in (Dehghan et al. 2013; Alcaraz et al. 2016). According to the conducted studies, to produce an appropriate temperature gradient in the SGSP containing the NaCl–water solution, this difference should be at least 0.216 g/cm³ (Kurt et al. 2000).

As can be seen in Fig. 7, due to the evaporation from the upper layer and the salt diffusion from the bottom layer to the upper layers, the salt concentration increased in the upper layers and decreased in the lower layers. These effects
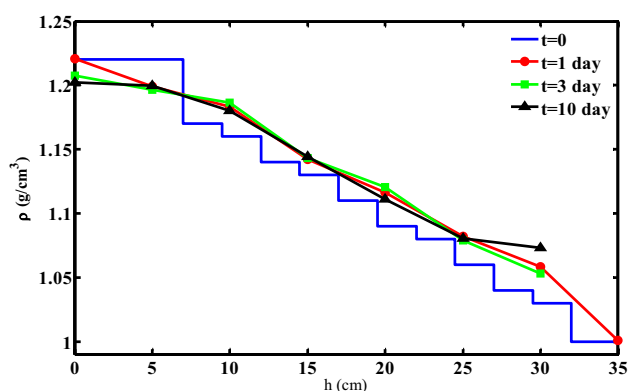
could lead to a reduction in the slope of the salinity gradient inside the pond.

After ensuring the stability of the saltwater layers, the solar pond was placed under the sun simulator light. At the specified time interval, the temperature in different layers was read and recorded. To ensure the stability testing of the pond, sampling was done from the saltwater solution by the sampling hoses, and the density and temperature were recorded for each sample.

Results and discussion

Figure 8 shows the changes in the temperature at various times throughout the solar pond. During the testing, due to the increase in the temperature of the pond layers and the evaporation phenomenon, the pond's water height was decreased from 35.7 cm to 29.3 cm. Hence, the evaporation rate from the SGSP surface was about 6.4 cm/day. To compensate for evaporation and to prevent salt concentration increase (via salt diffusion from the lower layers to the upper layers) at the solar pond surface, fresh water was gradually added to the pond using plastic piset and distributed via a sheet of expanded polystyrene (EPS) floating on the water surface when the fresh water was added. Since the pond was located in a laboratory setting, the surrounding temperature fluctuations during the test were about 2.5 °C. The pond temperature reached the steady state after 48 h of exposure to light.

Since the lamp was near the pond surface, with starting the test and turning on the lamp, the upper layer temperature was raised; then upon the passage of time, its temperature reached the stable conditions. Under steady-state conditions, the difference in temperature between the upper and lower layers of the pond was about 6.5 °C which is similar to what had been reported in (Kurt et al. 2006).

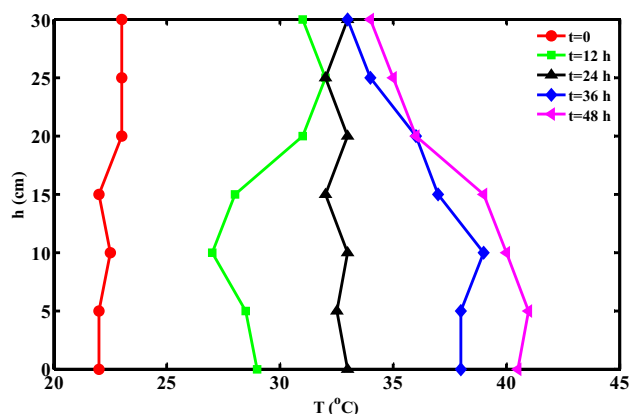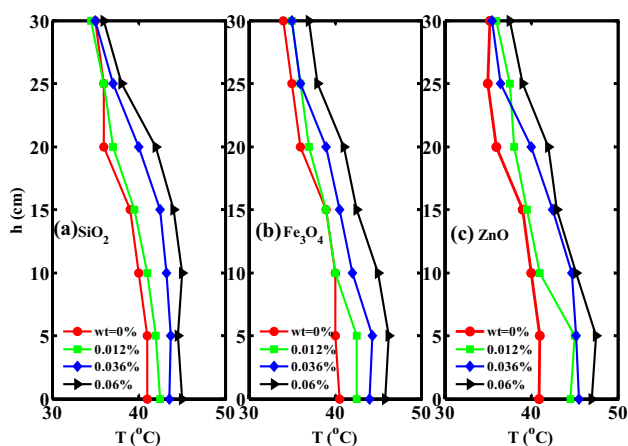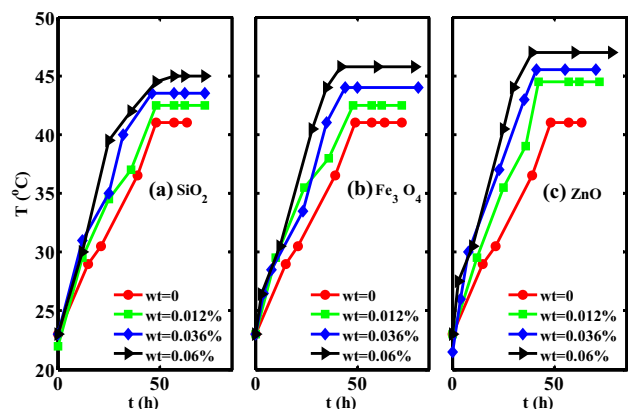**Fig. 7** Salinity gradient along the pond height

Fig. 8 Solar pond temperature distribution at various times

Fig. 9 Effect of nanoparticles on the storage layer temperature **a** SiO₂ nanoparticles, **b** Fe₃O₄ nanoparticles, and **c** ZnO nanoparticles

Fig. 10 Storage layer temperature vs. time for **a** SiO₂ nanofluids, **b** Fe₃O₄ nanofluids, and **c** ZnO nanofluids

The effect of the mentioned nanoparticles on the temperature distribution along pond is shown in Fig. 9. The effect of nanoparticles with the mass percentages of 0.012%, 0.036%, and 0.06% was studied. According to Fig. 9, the solar pond temperature increased with nanoparticles loading. At the same nanoparticles' concentration, ZnO nanoparticles had a better performance than other nanoparticles.

Figure 10 shows the changes in the LCZ temperature over time. According to the surrounding temperature, after about 48 h of light exposure, the LCZ temperature was increased; then, it was not changed by the passage of time. It could be seen that zinc oxide nanoparticles stored higher energy in the LCZ in comparison with other nanoparticles. By using ZnO, Fe₃O₄, and SiO₂ nanoparticles inside the LCZ, the maximum augmentation of the LCZ temperature in the nanofluids LCZ, as compared to the salt-water LCZ, was about 14.91%, 13.07%, and 9.75%, respectively.

The presence of nanoparticles inside the LCZ leads to an increase in its thermal conductivity. Therefore, the uniform temperature distribution is obtained in the LCZ, whereby heat transfer from the pond decreases. For this situation, the time to achieve thermal equilibrium conditions in the pond was decreased, with the maximum of about 9 h.

The intensity of artificial sunlight that reached the surface of the water column was decreased with increasing the depth. This decline was worse due to the presence of salinity and turbidity in water. Part of the light which penetrated into the saltwater was absorbed by the UCZ and NCZ layers and scattered due to the presence of the dissolved matter. When the particle size parameter (PSP) was much less than one, the scattering light portion was ignored. The PSP is written as

$$PSP = \frac{\pi d_p}{\lambda}, \tag{3}$$

where d_p is the nanoparticles average diameter (from DLS analysis) and λ is the wavelength. At the peak of absorption, the PSP for SiO₂, Fe₃O₄, and ZnO nanofluids was 0.488, 0.309, and 0.248, respectively. Hence, the ZnO nanofluids had the lowest PSP value among the studied nanofluids. As a result, it is expected that ZnO nanofluids absorb most of the light radiation.

Since the bottom of the SGSP was painted black, it could be assumed that a very little portion of light was reflected by the bottom wall. Therefore, the main portion of the light emitted into the pond was trapped by the LCZ, leading to the increase of the LCZ temperature.

The SGSP energy performance, said thermal efficiency, is defined as the ratio of energy storage in the LCZ during the experiment to the total energy reached to the LCZ in that time. According to the conducted studies (Ruskowitz et al. 2014), supposed that 68% of the total thermal energy fallen on the surface of the SGSP reached the LCZ–NCZ interface. Therefore, thermal efficiency is obtained by the following equation:

$$\eta = \frac{\rho A h c_p \Delta T}{0.68 \times G}, \tag{4}$$

where $\rho = 1.200$ g/cm³ is salt-water density, $A = 670$ cm² is the SGSP surface area, $h \approx 8$ cm is the depth of the LCZ, c_p is the specific heat capacity of the saltwater and calculated from Eq. 5, ΔT is the temperature difference between the start and the end of the test and $G \approx 5.1$ MJ is the total light radiation fallen on the SGSP surface during the test. Since the worst case was considered in the calculations, the smallest temperature difference, i.e., the difference between the minimum LZC temperature and the maximum ambient temperature, was used to calculate the thermal efficiency.

The specific heat capacity of saltwater can be determined as follows:

$$c_P = 4180 - 4.39\,c + 0.0048\,c^2, \tag{5}$$

where c is the salt concentration in kg/m^3.

Therefore, the thermal efficiency of the SGSP is $\eta = \frac{1.2 \times 670 \times 8 \times 3.446 \times 18.5}{0.68 \times 5.1 \times 10^6} = 0.1182$ or 11.82%. Thermal efficiency was obtained within a reasonable range and showed that the SGSP seems to operate well.

Thermal efficiency enhancement ratio is defined as the ratio of the SGSP thermal efficiency with nanofluids LCZ to that with salt-water LCZ:

$$E = \frac{\rho_{nf} c_{p_{nf}} \Delta T_{nf}}{\rho c_p \Delta T}, \tag{6}$$

where nanofluids properties (namely, density and specific heat capacity) can be calculated according to the following equations (Shahmohammadi and Beiki 2016):

$$\rho_{nf} = \varphi \rho_p + (1 - \varphi) \rho_{bf} \tag{7}$$

$$c_{p_{nf}} = \frac{\varphi (\rho c_p)_p + (1 - \varphi)(\rho c_p)_{bf}}{\rho_{nf}}, \tag{8}$$

where φ is the nanoparticles volume fraction, and subscripts nf, p, and bf refer to nanofluids, nanoparticles and based fluid. In this study, the based liquid is the saline solution.

The volume fraction of nanoparticles can be evaluated by the following formula:

$$\varphi = \frac{1}{1 + \frac{\rho_p}{\rho_{bf}}\left(\frac{1}{\omega_p} - 1\right)}, \tag{9}$$

where ω_p is the nanoparticles mass fraction.

The thermal efficiency enhancement ratios for different nanofluids, in all nanoparticles concentrations, are tabulated in Table 4 for comparison. In all concentrations, the thermal efficiency enhancement ratio for the ZnO nanofluids LCZ was greater than that for other nanofluids, thereby confirming that ZnO nanoparticles, among other nanoparticles, could be more effective to be applied in the solar ponds.

Finally, opaque ZnO nanofluids could have extraordinary optical properties, with a great potential to be used in the solar systems, especially in the solar ponds. This was because for this nanofluid, good stability, low light transparency and scattering, and the maximum time reduction to reach equilibrium were observed.

Table 4 Thermal efficiency enhancement ratio for various nanofluids

Nanoparticles type	Mass percentage (%)	Volume percentage (%)	E (%)
SiO$_2$	0.012	0.006	10.81
	0.036	0.018	16.20
	0.06	0.03	24.30
Fe$_3$O$_4$	0.012	0.003	8.11
	0.036	0.009	18.92
	0.06	0.014	28.64
ZnO	0.012	0.003	21.62
	0.036	0.008	27.02
	0.06	0.013	35.13

Conclusion

In this study, thermal energy storage in the LCZ of the small-scale laboratory SGSP was evaluated using a simple and inexpensive method. Three different types of nanofluids with various nanoparticles concentration were prepared by dispersing SiO$_2$, Fe$_3$O$_4$, and ZnO nanoparticles inside the saline water as hosing solution. The effect of the mentioned nanoparticles dispersion inside the LCZ, as well as the effect on the LCZ temperature and thermal efficiency of the SGSP was studied. After 3 days of filling the pond, the salinity gradient was formed and this gradient was stable. The salinity of the layers in the pond was maintained during the experiments. The thermal efficiency of the SGSP, without nanoparticles, was about 11.8%, showing that it had an excellent design and contracture. All nanofluids well-stable with maximum sedimentation of 16% after storage for 5 days at stagnant conditions. The nanofluids absorption and concentration showed the linear trend and consistent with the Beer–Lambert law. By increasing the nanoparticles concentration, the transparency of the nanofluids decreased, resulting in decreased transmittance. Using the mentioned nanofluids as the LCZ caused the LCZ temperature to be increased; subsequently, it could be concluded that more energy was stored in this layer. The maximum augmentation of the LCZ temperature in nanofluids compared to the based fluid was about 35.13% for 0.06% ZnO nanofluid. The thermal efficiency enhancement ratio increased with nanoparticles concentrations. As expected, the maximum enhancement ratio occurred for 0.06% ZnO nanofluid. By comparing the performance of the mentioned nanofluids, it could be concluded that among all nanofluids, 0.06% zinc oxide nanofluids was more effective. This was because this nanofluid with the opaque white color had nearly zero transmittance. The transmittance of 0.06% ZnO nanofluid was less than 4% over the UV–Vis spectrum. It could be said that the main part of the emitted light energy was absorbed with this nanofluid.

Compliance with ethical standards

Conflict of interest On behalf of all authors, the corresponding author states that there is no conflict of interest.

References

Abdullah AA, Lindsay KA, AbdelGawad AF (2016) Construction of sustainable heat extraction system and a new scheme of temperature measurement in an experimental solar pond for performance enhancement. Sol Energy 130:10–24. https://doi.org/10.1016/j.solener.2016.02.005

Alcaraz A, Valderrama C, Cortina JL, Akbarzadeh A, Farran A (2016) Enhancing the efficiency of solar pond heat extraction by using both lateral and bottom heat exchangers. Sol Energy 134:82–94. https://doi.org/10.1016/j.solener.2016.04.025

Al-Nimr MdA, Al-Dafaie AMA (2014) Using nanofluids in enhancing the performance of a novel two-layer solar pond. Energy 68:318–326. https://doi.org/10.1016/j.energy.2014.03.023

Assari MR, Basirat Tabrizi H, Kavoosi Nejad A, Parvar M (2015) Experimental investigation of heat absorption of different solar pond shapes covered with glazing plastic. Sol Energy 122:569–578. https://doi.org/10.1016/j.solener.2015.09.013

Banat F, El-Sayed S, El-Temtamy S (1994) Carnalite salt gradient solar ponds: an experimental study. Renew energy 4(2):265–269

Beiki H, Dadvar M, Halladj R (2009) Pore network model for catalytic dehydration of methanol at particle level. AIChE J 55(2):442–449

Beiki H, Esfahany M, Etesami N (2013a) Turbulent mass transfer of Al2O3 and TiO2 electrolyte nanofluids in circular tube. Microfluid Nanofluid 15(4):501–508. https://doi.org/10.1007/s10404-013-1167-z

Beiki H, Nasr Esfahany M, Etesami N (2013b) Laminar forced convective mass transfer of γ-Al2O3/electrolyte nanofluid in a circular tube. Int J Therm Sci 64(0):251–256. https://doi.org/10.1016/j.ijthermalsci.2012.09.004

Bozkurt I, Deniz S, Karakilcik M, Dincer I (2015) Performance assessment of a magnesium chloride saturated solar pond. Renew Energy 78:35–41. https://doi.org/10.1016/j.renene.2014.12.060

Chen W, Zou C, Li X, Li L (2017) Experimental investigation of SiC nanofluids for solar distillation system: stability, optical properties and thermal conductivity with saline water-based fluid. Int J Heat Mass Transf 107:264–270. https://doi.org/10.1016/j.ijheatmasstransfer.2016.11.048

Dehghan AA, Movahedi A, Mazidi M (2013) Experimental investigation of energy and exergy performance of square and circular solar ponds. Sol Energy 97:273–284. https://doi.org/10.1016/j.solener.2013.08.013

Elsarrag E, Igobo ON, Alhorr Y, Davies PA (2016) Solar pond powered liquid desiccant evaporative cooling. Renew Sustain Energy Rev 58:124–140. https://doi.org/10.1016/j.rser.2015.12.053

Fard MM, Beiki H (2017) Experimental measurement of solid solutes solubility in nanofluids. Heat Mass Transfer 53(4):1257–1263. https://doi.org/10.1007/s00231-016-1894-2

Gulzar O, Qayoum A, Gupta R (2018) Photo-thermal characteristics of hybrid nanofluids based on Therminol-55 oil for concentrating solar collectors. Appl Nanosci. https://doi.org/10.1007/s13204-018-0738-4

Hassairi M, Safi M, Chibani S (2001) Natural brine solar pond: an experimental study. Sol Energy 70(1):45–50

Karakilcik M, Kıymac K, Dincer I (2006) Experimental and theoretical temperature distributions in a solar pond. Int J Heat Mass Transf 49(5):825–835

Karunamurthy K, Murugumohankumar K, Suresh S (2012) Use of CuO nano-material for the improvement of thermal conductivity and performance of low temperature energy storage system of solar pond. Digest J Nanomater Biostructures 7(4):1833–1841

Karuppuchamy S, Andou Y, Endo T (2013) Preparation of nanostructured TiO2 photoelectrode for flexible dye-sensitized solar cell applications. Appl Nanosci 3(4):291–293. https://doi.org/10.1007/s13204-012-0140-6

Keramati M, Beiki H (2017) The effect of pH adjustment together with different substrate to inoculum ratios on biogas production from sugar beet wastes in an anaerobic digester. J Energy Manag Technol 1(2):6–11

Keren Y, Rubin H, Atkinson J, Priven M, Bemporad G (1993) Theoretical and experimental comparison of conventional and advanced solar pond performance. Sol Energy 51(4):255–270

Kho T, Hawlader M, Ho J, Wijeysundera N (1991) Design and performance evaluation of a solar pond for industrial process heating. Int J Solar Energy 10(1–2):83–101

Kurt H, Halici F, Binark AK (2000) Solar pond conception—experimental and theoretical studies. Energy Convers Manag 41(9):939–951

Kurt H, Ozkaymak M, Binark AK (2006) Experimental and numerical analysis of sodium-carbonate salt gradient solar-pond performance under simulated solar-radiation. Appl Energy 83(4):324–342

Ladjevardi S, Asnaghi A, Izadkhast P, Kashani A (2013) Applicability of graphite nanofluids in direct solar energy absorption. Sol Energy 94:327–334

Leshuk J, Zaworski R, Styris D, Harling O (1978) Solar pond stability experiments. Sol Energy 21(3):237–244

Li XY, Kanayama K, Baba H (2000) Spectral calculation of the thermal performance of a solar pond and comparison of the results with experiments. Renew Energy 20(4):371–387

Liu H, Jiang L, Wu D, Sun W (2015) Experiment and simulation study of a trapezoidal salt gradient solar pond. Sol Energy 122:1225–1234. https://doi.org/10.1016/j.solener.2015.09.006

Lund P, Keinonen R (1984) Radiation transmission measurements for solar ponds. Sol Energy 33(3):237–240

Mahian O, Kianifar A, Kalogirou SA, Pop I, Wongwises S (2013) A review of the applications of nanofluids in solar energy. Int J Heat Mass Transf 57(2):582–594. https://doi.org/10.1016/j.ijheatmasstransfer.2012.10.037

Manouchehrian Fard M, Beiki H (2016) Experimental investigation of benzoic acid diffusion coefficient in γ-Al2O3 nanofluids at different temperatures. Heat Mass Transfer 52(10):2203–2211. https://doi.org/10.1007/s00231-015-1734-9

Michael JJ, Iniyan S (2015) Performance of copper oxide/water nanofluid in a flat plate solar water heater under natural and forced circulations. Energy Convers Manag 95:160–169. https://doi.org/10.1016/j.enconman.2015.02.017

Milanese M, Colangelo G, Cretì A, Lomascolo M, Iacobazzi F, de Risi A (2016) Optical absorption measurements of oxide nanoparticles for application as nanofluid in direct absorption solar power systems–Part II: ZnO, CeO2, Fe2O3 nanoparticles behavior. Sol Energy Mater Sol Cells 147:321–326

Murthy GR, Pandey K (2003) Comparative performance evaluation of fertiliser solar pond under simulated conditions. Renew Energy 28(3):455–466

Pawar S, Chapgaon A (1995) Fertilizer solar ponds as a clean source of energy: some observations from small scale experiments. Sol Energy 55(6):537–542

Qarony W, Hossain MI, Jovanov V, Knipp D, Tsang YH (2018) Maximizing the short circuit current of organic solar cells by partial

decoupling of electrical and optical properties. Appl Nanosci 8(3):339–346. https://doi.org/10.1007/s13204-018-0713-0

Rajaseenivasan T, Murugavel KK, Elango T, Hansen RS (2013) A review of different methods to enhance the productivity of the multi-effect solar still. Renew Sustain Energy Rev 17:248–259. https://doi.org/10.1016/j.rser.2012.09.035

Rashidi S, Esfahani JA, Rashidi A (2017) A review on the applications of porous materials in solar energy systems. Renew Sustain Energy Rev 73:1198–1210. https://doi.org/10.1016/j.rser.2017.02.028

Rativa D, Gómez-Malagón LA (2015) Solar radiation absorption of nanofluids containing metallic nanoellipsoids. Sol Energy 118:419–425. https://doi.org/10.1016/j.solener.2015.05.048

Rose BAJ, Singh H, Verma N, Tassou S, Suresh S, Anantharaman N, Mariotti D, Maguire P (2017) Investigations into nanofluids as direct solar radiation collectors. Sol Energy 147:426–431. https://doi.org/10.1016/j.solener.2017.03.063

Ruskowitz JA, Suárez F, Tyler SW, Childress AE (2014) Evaporation suppression and solar energy collection in a salt-gradient solar pond. Sol Energy 99:36–46

Said Z, Sajid M, Alim M, Saidur R, Rahim N (2013) Experimental investigation of the thermophysical properties of Al$_2$O$_3$-nanofluid and its effect on a flat plate solar collector. Int Commun Heat Mass Transfer 48:99–107

Salata F, Coppi M (2014) A first approach study on the desalination of sea water using heat transformers powered by solar ponds.

Appl Energy 136:611–618. https://doi.org/10.1016/j.apenergy.2014.09.079

Shahmohammadi P, Beiki H (2016) A numerical investigation of γ-Al$_2$O$_3$-water nanofluids heat transfer and pressure drop in a shell and tube heat exchanger. Transp Phenom Nano Micro Scales 4(1):29–35

Subhakar D, Murthy SS (1991) Experiments on a magnesium chloride saturated solar pond. Renew Energy 1(5–6):655–660

Subhakar D, Murthy SS (1994) Saturated solar ponds: 3. Experimental verification. Sol Energy 53(6):469–472

Tsilingiris PT (1996) Design and performance of large low-cost solar water heating systems. Renew Energy 9(1):617–621. https://doi.org/10.1016/0960-1481(96)88364-9

Tyagi H, Phelan P, Prasher R (2009) Predicted efficiency of a low-temperature nanofluid-based direct absorption solar collector. J Solar Energy Eng 131(4):041004

Ziapour BM, Shokrnia M, Naseri M (2016) Comparatively study between single-phase and two-phase modes of energy extraction in a salinity-gradient solar pond power plant. Energy 111:126–136. https://doi.org/10.1016/j.energy.2016.05.114

Springer